

Role of Cation Polarization in *holo*- and *hemi*-Directed $[\text{Pb}(\text{H}_2\text{O})_n]^{2+}$ Complexes and Development of a Pb^{2+} Polarizable Force Field

Mike Devereux,^{*,†} Marie-Céline van Severen,[‡] Olivier Parisel,[‡]
Jean-Philip Piquemal,^{*,‡,§} and Nohad Gresh^{*,†}

Université Paris Descartes, Laboratoire de Chimie et Biochimie Pharmacologiques et Toxicologiques, UMR 8601 CNRS, UFR Biomédicale, 45 rue des Saints-Pères, 75270 Paris Cedex06, France; UPMC, Université Paris 06, UMR 7616, Laboratoire de Chimie Théorique, Case Courrier 137, 4 Place Jussieu, F-75005 Paris, France; and CNRS, UMR 7616, Laboratoire de Chimie Théorique, case courrier 137, 4 place Jussieu, F-75005 Paris, France

Received July 19, 2010

Abstract: Reduced Variational Space (RVS) calculations are reported that afford insight into the energetic origins of the *hemi*- and *holo*-directing behavior of $[\text{Pb}(\text{H}_2\text{O})_n]^{2+}$ complexes. It is shown that the distribution of ligands around the Pb^{2+} center arises from a delicate balance between the first-order Coulomb plus exchange-repulsion energy that favors *holo*-directionality, and the second-order charge transfer plus polarization term that favors *hemi*-directionality. It is additionally demonstrated that the pseudopotential/basis set combination used to study such complexes should be carefully selected, as artifacts can arise when using large-core pseudo-potentials. Finally, based on these findings, we introduce a new SIBFA force field parametrization for Pb^{2+} . Results yield close agreement with ab initio complexation energies in a series of $[\text{Pb}(\text{H}_2\text{O})_n]^{2+}$ complexes and successfully encapsulate the *hemi*- and *holo*-directing properties. SIBFA thus appears to be the first classical force field to be able to model the *holo*-/*hemi*-directed transition within Pb complexes, avoiding the need for explicit wave function treatment and consequently providing the opportunity to deal with large leaded systems of biological interest.

Introduction

As lead is an abundant metal that is easily extracted and has a low melting point and high malleability, it has been widely used for everything from making cooking utensils, paints, or water pipes to electrochemical cells, and as an additive to gasoline in internal combustion engines. As a result, it has become widely dispersed in the environment,¹ and due

to the high toxicity associated with Pb^{2+} , poses a significant threat to human health.² Pb accumulated in the body causes lead poisoning, or saturnism, an intoxication that is especially severe among children³ and threatens many people in developing nations where contact with lead-contaminated soils and drinking water is most common.⁴

Lead is easily oxidized to form Pb^{2+} aquocations. Pb^{2+} then competes with and displaces native cations such as Zn^{2+} in important proteins such as Aminolevulinic Acid Dehydratase (ALAD),^{5–9} inhibiting normal protein function. Explaining the affinity and structural changes associated with binding of Pb^{2+} in complex biological environments and designing chelating agents that are able to selectively extract Pb^{2+} in preference to other metal cations is a particularly challenging task.¹⁰ The high atomic number of Pb^{2+} ($Z =$

* To whom correspondence should be addressed. E-mail: mike.devereux@parisdescartes.fr; nohad.gresh@parisdescartes.fr; jpp@lct.jussieu.fr.

† Université Paris Descartes, U648 INSERM, UFR Biomédicale.

‡ Université Pierre et Marie Curie—Paris 06, UMR 7616, Laboratoire de Chimie Théorique.

§ CNRS, UMR 7616, Laboratoire de Chimie Théorique.

82) makes full-electron, relativistic ab initio calculations prohibitive for all but the smallest complexes. There is also an unusual tendency of Pb^{2+} complexes to switch between even spacing of ligands around the metal center in a so-called *holo*-directed conformation, and a second class of structures where ligands are directed to one side of the metal in a sterically crowded *hemi*-directed conformation. The preference for *holo*- or *hemi*-directionality depends on many parameters, such as the number of coordinating ligands and resulting steric crowding, the ligand flexibility, and additional repulsion between ligands that carry a formal charge.¹¹ The reason Pb^{2+} exhibits this unusual behavior is often attributed to a sterically active lone-pair,^{12,13} making it difficult to model using traditional classical force fields. The availability of a reliable molecular mechanics approach would allow studies of Pb^{2+} binding with greater conformational sampling and in more complex environments than those currently accessible by means of electronic structure methods.

As force fields typically combine separate energetic terms to estimate the total interaction energy between moieties, a deeper understanding of the energetic contributions favoring *holo* and *hemi* orientation in different complexes is an important first step toward parametrizing a reliable force field. One methodology that can be applied in this context is the Reduced Variational Space (RVS) scheme of Stevens and Fink.¹⁴ RVS decomposes the total ab initio interaction energy between fragments into first-order Coulomb and Pauli-repulsion terms, and second-order polarization and charge-transfer components. All of these contributions are accounted for using approximate expressions in the SIBFA (Sum of Interactions Between Fragments Ab initio computed) polarizable force field.^{15–19} As a result, RVS has been successfully used for the energetic decomposition of various systems including Zn^{2+} -complexes,²⁰ water clusters²¹ and hard and soft metal cations,²² to allow parametrization of SIBFA and for subsequent evaluation of force field accuracy.

SIBFA is a detailed, fragment-based force field that has been widely applied to proteins and organometallic systems, from small complexes to proteins/metalloproteins^{23–26} (see ref 19 for a detailed review article). The force field energetic terms explicitly account for anisotropic fragment polarization, repulsion, and charge transfer, as well as for distributed multipole moments centered at both nuclear positions and bond barycenters. While computationally more expensive than many popular classical force fields such as CHARMM²⁷ and AMBER,²⁸ SIBFA yields molecular structures and energies that are generally in close agreement with ab initio data while maintaining a much lower computational overhead than would be required for a full ab initio computation. Although the interest in polarizable, anisotropic force fields has recently grown,^{29–31} SIBFA remains one of the most developed and widely applied. Parameters exist for a wide range of organic compounds and closed-shell organometallic systems that contain metals such as Mg(II), Ca(II), Zn(II), and Cd(II). A recent extension, “SIBFA-LF”, includes ligand field effects by means of the angular overlap model^{32,33} (AOM) and has allowed extension of the range of applications to transition metal cations with partially filled *d*-shells, such as Cu(II).¹⁵ In addition, short-range energetic corrections

allow SIBFA to describe the formation of ligand–metal complexes without resorting to separate bonded and non-bonded parameters. A single, consistent parameter set can thus be used to explore for example binding, dissociation and relative energies of different tautomers and conformers. The goal of the current work is to use information gained about the formation of Pb^{2+} -complexes from RVS calculations to extend the range of application of SIBFA to Pb^{2+} compounds, offering a capability for molecular mechanics to model the *holo*- to *hemi*-directing transition.

Computational Procedures

Electronic Structure Calculations. To explore the performance of different pseudopotentials, $[\text{Pb}(\text{H}_2\text{O})_n]^{2+}$ complexes were geometry-optimized using the Gaussian03 program³⁴ at the restricted Hartree–Fock (RHF) and B3LYP^{35,36} levels of theory. Four different pseudopotential (PP)/basis set combinations were tested. Three large-core PPs were used: the Stuttgart relativistic large-core PP³⁷ (henceforth SDD), the large-core relativistic PP of Ross and co-workers³⁸ (henceforth CRENS), and for consistency with previous SIBFA parametrization studies, the SBK compact relativistic PP.³⁹ Basis sets and PPs for Pb were taken from the Basis Set Exchange^{40,41} and are included as Supporting Information. Remaining atom types were described using a 6-31+G** basis set for the SDD and CRENS PPs, as successfully applied in previous work on $[\text{Pb}(\text{H}_2\text{O})]^{2+}$.⁴² SBK calculations employed an effective core potential for oxygen atoms⁴³ with a CEP 4–31G(2d) basis set for both oxygen and hydrogen. For comparison, a small-core relativistic PP of Peterson,⁴⁴ designed for use with aug-cc-pVnZ basis sets was selected and used with a triple- ζ basis set for lead and remaining atoms. Binding energies were evaluated as the difference in energy between the bound complex and isolated, geometry-optimized monomers.

Comparison of the performance of different ab initio and DFT methods was carried out similarly using the small-core PP of Peterson with aug-cc-pVTZ basis set for Pb^{2+} and bound ligands. The DFT methods tested with this PP/basis set combination were the M05–2X,⁴⁵ M06,⁴⁶ B3LYP,^{35,36,47} and PBE^{48,49} density functionals available in Gaussian03.³⁴ Restricted Hartree–Fock, CCSD,^{50,51} CCSD(T),⁵² and MP2^{53,54} calculations were performed with the same PP and aug-cc-pVTZ basis set. Finally, the $[\text{Pb}(\text{H}_2\text{O})]^{2+}$ monohydrated complex was geometry-optimized with each method using a larger aug-cc-pVQZ basis set and with the same small-core PP. This PP/quadruple- ζ basis set combination was additionally used with B3LYP to optimize $[\text{Pb}(\text{H}_2\text{O})_n]^{2+}$ complexes ($n = 1, 2, 4$).

RVS calculations were performed using Gamess⁵⁵ to decompose the RHF interaction energy. The RVS procedure is related to Morokuma decomposition⁵⁶ but maintains the antisymmetry of the wave function, and in this respect is similar to the Constrained Space Orbital Variation (CSOV) method of Bagus.⁵⁷ PPs and basis sets used in Gamess were again taken from the Basis Set Exchange.

The Electron Localization Function (ELF), originally proposed by Becke and Edgecombe⁵⁸ offers useful insight

into the effect of complexation on the behavior of the Pb^{2+} lone-pair. The basin associated with the lone pair $V(\text{Pb})$ is obtained by topological analysis to allow both quantitative study and visualization of the basin's position and shape.^{58–64} In the present contribution, the ELF calculations and their analysis were performed using a modified version of the TOPMOD package^{59,65,66} with electronic densities calculated by Gaussian03.

SIBFA. The SIBFA force field has been described in detail elsewhere,^{15–17,19,24,67} only a brief overview will be given here with additional details available as Supporting Information. SIBFA is an anisotropic, polarizable force field in which molecules are broken down into rigid fragments that are free to rotate about their connection points (torsional degrees of freedom). Both inter- and intramolecular energies are evaluated as the sum of interactions between constituent chemical fragments. Unusually for a force field, SIBFA explicitly accounts for electrostatic (E_{mnp}), repulsion (E_{rep}), charge-transfer (E_{ct}), and polarization (E_{pol}) energies in evaluating the total interaction energy ΔE_{tot} :

$$\Delta E_{\text{tot}} = E_{\text{mnp}} + E_{\text{rep}} + E_{\text{pol}} + E_{\text{ct}} + E_{\text{disp}} \quad (1)$$

The final term " E_{disp} " represents an estimation of the dispersion energy to afford improved agreement with post-HF methodologies.⁶⁷

The electrostatic term E_{mnp} is evaluated using a multipole expansion, with both atom- and bond-centered multipole moments included up to quadrupole. Multipole moments are derived from the ab initio charge density according to the procedure of Vigné-Maeder and Claverie.⁶⁸ The sharing of multipoles between both atoms and bond centers ensures improved short-range convergence. A recently extended formulation¹⁸ adds a penetration contribution to account for the overlap of molecular charge densities, further improving evaluation of short-range electrostatic interactions.

The short-range repulsion term E_{rep} accounts for Pauli-repulsion between same-spin electrons, and is modeled in SIBFA by means of a sum of bond–bond, bond–lone pair and lone pair–lone pair interactions. Bond sites are located at the barycenters between bonded atoms within a fragment. The positions of electron lone pairs are defined using Boys localization of orbital centroids.^{69–71} Use of bonds and lone-pairs in place of atom-centered repulsion sites allows increased anisotropy and a more accurate representation of the repulsion energy.^{24,67}

The charge transfer term E_{ct} is especially important where metal–ligand bonds exhibit some degree of covalent character. Electron density from the bound ligands can be transferred to the central metal cation M , and back-donation to or from the d -orbitals of transition metals can provide an additional energetic contribution.^{17,72,73} Charge transfer in SIBFA is evaluated by approximating orbital overlap using the distance and angles between localized lone pair orbitals of the interacting entities.^{17,72,74,75}

Polarization of the fragments' electron density makes the final major contribution to the total interaction energy in the standard SIBFA force field. The polarizability tensors are located on the centroids of the Boys localized orbitals (chemical bonds and heteroatom lone pairs). They are derived

from the quantum chemical wave function of each fragment using a procedure developed by Garmer and Stevens.⁶⁹ Recent data show that, if off-centered lone pair polarizabilities are explicitly represented, classical polarizable force fields can afford a close agreement with the ab initio results, both in terms of polarization energy and in terms of dipole moment (see ref 71 for details). The polarization energy takes the form of an interaction between an induced dipole and the electric field generated by surrounding moieties; for metal cations an additional induced quadrupole interacting with the field gradient is considered (see references 19, 75 and references therein). A Gaussian screening term intervenes in the evaluation of the electric field arising from a given multipolar site at very close range to prevent close contact between charge-carrying sites of one moiety and polarizable sites of another, which could give rise to unphysically large polarization energies.^{17,24}

Results

Pseudo-Potential Comparison. A series of $[\text{Pb}(\text{H}_2\text{O})_n]^{2+}$ clusters ($1 \leq n \leq 6$) were energy-minimized using the SDD, CRENBS, and SBK large-core PPs, as well as using one small-core PP with aug-cc-pVTZ basis set. Binding enthalpies of Pb^{2+} were calculated as described in the Methods section. In the case of the hexacoordinated $[\text{Pb}(\text{H}_2\text{O})_6]^{2+}$ complex two stable structures were found (Figure 1). The *holo*-directed $[\text{Pb}(\text{H}_2\text{O})_6]^{2+}$ structure was found to be a stable minimum at both Hartree–Fock and B3LYP levels of theory (confirmed by frequency calculations) with all PPs. The *hemi*-directed structure was found to be a stable minimum using the Hartree–Fock method with all PPs, and with B3LYP when using all PPs except the small-core PP with aug-cc-pVTZ basis set. Additional MP2 optimizations with the small-core PP and aug-cc-pVTZ basis set did find a stable minimum, however, so the MP2 geometry of the *hemi*-directed structure was used to perform B3LYP single point calculations for comparison with the other methods. ELF isosurfaces are shown in Figure 1 to illustrate topological features of the sterically active Pb^{2+} lone pair upon the transition from the *holo* to the *hemi*-directed structure of $[\text{Pb}(\text{H}_2\text{O})_6]^{2+}$. Similar plots for $[\text{Pb}(\text{CO})_5]^{2+}$ and $[\text{Pb}(\text{CO})_6]^{2+}$ are provided as Figure S1 in Supporting Information and in previous work.⁷⁶

Table 1 shows a comparison of the performance of the different PPs against previously published full-electron, four-component results for the $[\text{Pb}(\text{H}_2\text{O})]^{2+}$ complex.⁴² It can be seen that, while the small-core PP performs slightly better, SDD and CRENBS PPs also offer good agreement with the four-component results. SBK B3LYP results afford similar accuracy to CRENBS and SDD, although the binding energy is overestimated. The largest error of 6 kcal/mol arises with SBK and RHF. Pb–O distances are in good agreement for all PPs.

The final two columns of Table 1 show a comparison of binding energies using different PPs for the *holo*- and *hemi*-directed $[\text{Pb}(\text{H}_2\text{O})_6]^{2+}$ clusters. There is now significant quantitative disagreement in the Pb^{2+} binding energy, ranging, for example, from -207.7 kcal/mol for the *hemi*-directed structure with the SDD PP combined with B3LYP

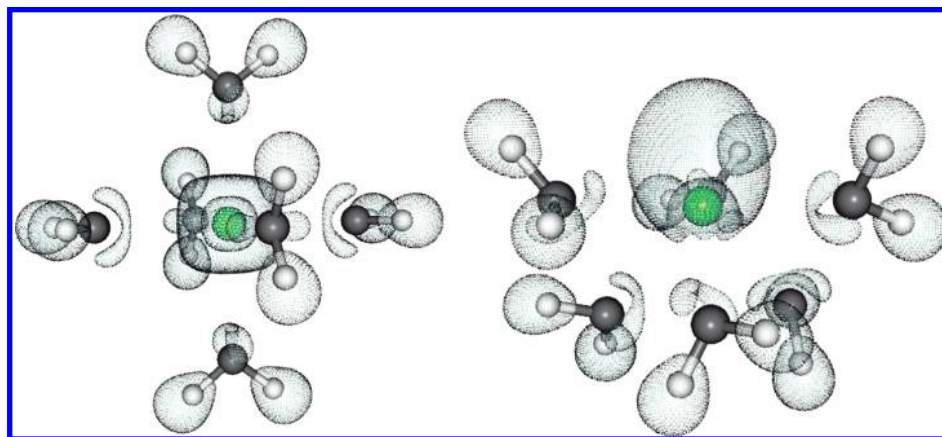


Figure 1. ELF isosurfaces ($\eta = 0.085$) showing the Pb^{2+} lone pair basin $V(\text{Pb})$ in *holo*- (left) and *hemi*-directed (right) $[\text{Pb}(\text{H}_2\text{O})_6]^{2+}$ structures. Pb^{2+} is shown in green with $V(\text{Pb})$ localized in the surrounding volume.

Table 1. Comparison of Binding Energy and Pb–O Distance (Å) in the $[\text{Pb}(\text{H}_2\text{O})]^{2+}$ Complex, and Binding Energies in *holo*- and *hemi*-Directed $[\text{Pb}(\text{H}_2\text{O})_6]^{2+}$ Complexes Using Different Pseudopotentials

pseudopotential	method	$[\text{Pb}(\text{H}_2\text{O})]^{2+}$ (BSSE corr)		$(\text{H}_2\text{O})_6$ <i>hemi</i>	$(\text{H}_2\text{O})_6$ <i>holo</i>
		$r(\text{Pb}-\text{O})$	ΔE (kcal/mol)	ΔE (kcal/mol)	ΔE (kcal/mol)
SBK	RHF	2.320	-59.5	-238.1	-234.5
	B3LYP	2.283	-66.8	-254.8	-252.0
CRENBS	RHF	2.388	-51.1	-207.3	-207.6
	B3LYP	2.367	-56.1	-218.5	-219.3
SDD	RHF	2.384	-49.9	-197.6	-197.8
	B3LYP	2.359	-55.0	-207.7	-208.2
aug-cc-pVTZ	RHF	2.336	-51.9	-198.5	-197.8
	B3LYP	2.322	-58.5	-211.6	-215.0
full- e^- relativistic ^a	DHF	2.347	-53.5		
	DB3LYP	2.338	-61.0		

^a Values taken from earlier work of Gourlaouen et al.⁴²

to -254.8 kcal/mol for the same complex with the SBK PP and B3LYP. Significantly, the predicted relative energies of the *holo*- and *hemi*-directed structures also differ. While the small-core PP suggests that the *holo*-directed structure is around 3.4 kcal/mol more stable than the *hemi*-directed structure, SDD and CRENBS with B3LYP predict the *holo*-directed structure to be approximately iso-energetic with the *hemi*-directed conformation. In contrast, SBK predicts the *hemi*-directed structure to be 2.8 kcal/mol more stable than the *holo* arrangement. The PP chosen therefore has a non-negligible impact on both the magnitude of the binding energy and the relative energies of different *holo*- and *hemi*-directed conformations of the same complex, necessitating careful selection.

Final selection of an appropriate PP was made on the basis of RVS data. Figure 2 shows the RVS Coulomb and repulsion energies in the $[\text{Pb}(\text{H}_2\text{O})]^{2+}$ complex as a function of Pb–O distance. While the Coulomb energy becomes exponentially more attractive with decreasing ligand-cation distance using the small-core PP, as should intuitively be the case, the large-core PPs cause artifacts to arise at short distance as the electron density of the ligand begins to overlap the effective core potential. The divergence between data from large and small core PPs starts to occur at around 2.4 Å, the optimized bond length in many of the Pb– H_2O complexes. The repulsion energy is also significantly lower at short-range using the large-core PPs than using the small-core PP. This leads to some cancellation of errors with the

correspondingly lower Coulomb contribution, but divergence in the repulsion energy starts at longer range than divergence in the Coulomb energy (about 2.6 Å). As the small-core PP affords the best agreement with four-component calculations for the $[\text{Pb}(\text{H}_2\text{O})]^{2+}$ complex and appears free from artifacts arising from ligand-PP core overlap at the distances of interest, it was selected to provide reference data for the series of $[\text{Pb}(\text{H}_2\text{O})_n]^{2+}$ complexes.

Ab Initio/Density Functional Method Comparison.

Having selected the small-core PP with aug-cc-pVTZ basis set, the stability of data to changes in electronic structure method was next investigated. Results are presented in Table 2. The less computationally expensive DFT methodologies were applied to all systems up to $[\text{Pb}(\text{H}_2\text{O})_5]^{2+}$, whereas CCSD optimizations were only possible up to $[\text{Pb}(\text{H}_2\text{O})_2]^{2+}$, and CCSD(T) was only possible for the $[\text{Pb}(\text{H}_2\text{O})]^{2+}$ complex with this PP/basis set combination. The table shows that all methods yield similar results. In particular, all DFT methods agree closely with one another. They afford complex formation energies around 3 kcal/mol lower than CCSD and CCSD(T) results for the $[\text{Pb}(\text{H}_2\text{O})]^{2+}$ complex, with MP2 results lying between the two. Hartree–Fock binding energies are somewhat underestimated with respect to the other methods. The close agreement between DFT and MP2 results is also visible for the larger clusters, suggesting that choice of electronic structure method has a smaller impact on calculated binding energies than the choice of PP.

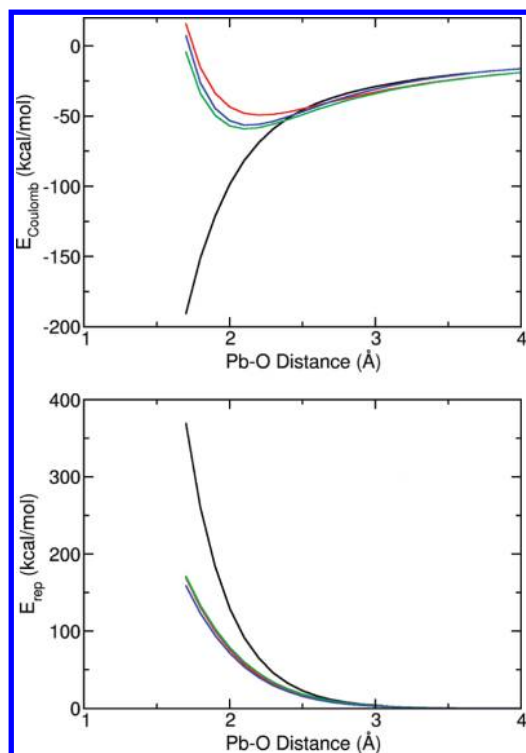


Figure 2. Coulomb (top) and repulsion (bottom) RVS contributions to the total interaction energy using different pseudopotentials: small-core with aug-cc-pVTZ (black), SDD (red), CRENSB (green), and SBK (blue) pseudopotentials with different basis sets are compared (see text for details).

Table 2. Comparison of $[\text{Pb}(\text{H}_2\text{O})_n]^{2+}$ Complex Formation Energies Relative to Gas Phase Monomer Energies Using the aug-cc-pVTZ Small-Core Pseudopotential and Basis Set with Different ab Initio and Density Functional Methods^a

$[\text{Pb}(\text{H}_2\text{O})]^{2+}$	$[\text{Pb}(\text{H}_2\text{O})_2]^{2+}$	$[\text{Pb}(\text{H}_2\text{O})_4]^{2+}$	$[\text{Pb}(\text{H}_2\text{O})_5]^{2+}$	
RHF	-51.9	-95.0	-157.8	-180.4
B3LYP pVTZ	-58.5	-105.5	-171.6	-195.4
B3LYP pVQZ	-58.8	-106.0	-172.2	-
M05-2X	-59.3	-108.4	-180.5	-206.9
M06	-58.6	-106.9	-177.9	-204.0
PBE	-59.3	-107.4	-175.8	-200.1
MP2	-56.6	-103.5	-172.4	-197.9
CCSD	-55.3	-100.6		
CCSD(T)	-55.7			
full e ⁻ DB3LYP ^b	-61.0			

^a The same pseudopotential with a larger aug-cc-pVQZ basis set is also shown. ^b Values taken from earlier work of Gourlaouen et al.⁴⁰

Finally, the convergence of the basis set was examined further by running a limited number of optimizations using the larger aug-cc-pVQZ basis set with B3LYP and the small-core PP. Again, little change in binding energies is observed, with differences between the aug-cc-pVTZ and aug-cc-pVQZ results generally within 1 kcal/mol. Similar results (not shown) were obtained using this basis set and the other electronic structure methods for the monohydrated complex. The B3LYP method with aug-cc-pVTZ basis set therefore appears to represent an acceptable level of theory to provide reference data for subsequent force field parametrization. In

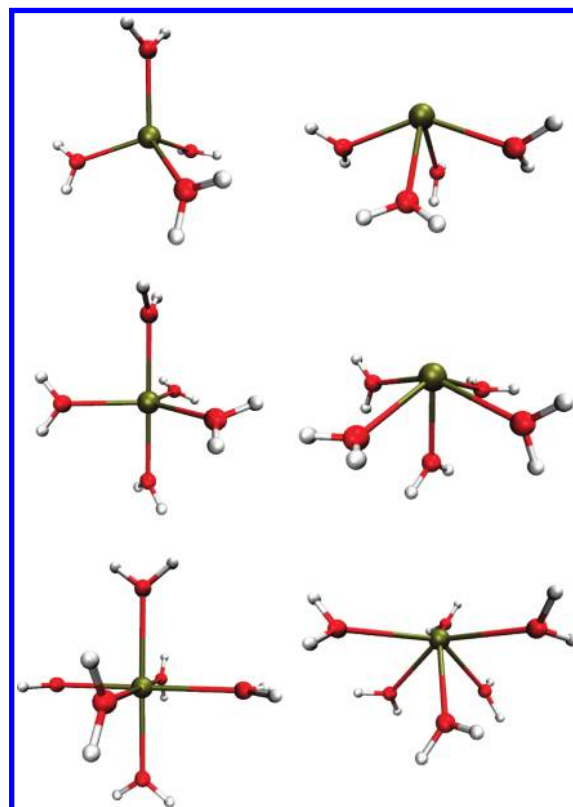


Figure 3. $[\text{Pb}(\text{H}_2\text{O})_4]^{2+}$ (top), $[\text{Pb}(\text{H}_2\text{O})_5]^{2+}$ (middle) and $[\text{Pb}(\text{H}_2\text{O})_6]^{2+}$ (bottom) *holo*- and *hemi*-directed structures used to investigate the energetic origins of *holo*- and *hemi*-directionality.

addition to good agreement with other methods tested here, it has been widely applied to the many organic ligands that will be of interest when applying the force field to studies of biological systems.

RVS Analysis of *holo*- and *hemi*-Directed Structures.

The energetic origins of the stabilization of *hemi*-directed complexes over their *holo*-directed counterparts were next investigated using RVS analysis. A series of $[\text{Pb}(\text{H}_2\text{O})_4]^{2+}$, $[\text{Pb}(\text{H}_2\text{O})_5]^{2+}$, and $[\text{Pb}(\text{H}_2\text{O})_6]^{2+}$ complexes were selected for study (Figure 3). The energy-minimized *hemi*-directed structures of all complexes obtained with the small-core PP and aug-cc-pVTZ basis set and B3LYP method were used, although, as already stated, an MP2 geometry had to be taken for $[\text{Pb}(\text{H}_2\text{O})_6]^{2+}$ as no stable *hemi*-directed structure was found for this complex using a small-core PP with B3LYP. The *holo*-directed structure of $[\text{Pb}(\text{H}_2\text{O})_6]^{2+}$ was used for comparison with the *hemi*-directed structure, along with an artificially created tetrahedral $[\text{Pb}(\text{H}_2\text{O})_4]^{2+}$ complex and a trigonal-bipyramidal $[\text{Pb}(\text{H}_2\text{O})_5]^{2+}$ structure that were obtained by constrained optimization of Pb-ligand bond lengths. These artificial *holo*-directed structures were created to allow direct RVS comparison for each complex between a *holo*- and the corresponding *hemi*-directed ligand arrangement.

The results of the RVS analysis are shown in Table 3. Interestingly, in all three complexes the lower ligand–ligand repulsion energy associated with the *holo*-directed complexes more than compensates for the slightly lower Coulomb energy, meaning that the total first-order con-

Table 3. RVS Energy Decomposition of *holo*- and *hemi*-Directed Structures of $[\text{Pb}(\text{H}_2\text{O})_4]^{2+}$, $[\text{Pb}(\text{H}_2\text{O})_5]^{2+}$, and $[\text{Pb}(\text{H}_2\text{O})_6]^{2+}$ Complexes (kcal/mol)

$[\text{Pb}(\text{H}_2\text{O})_4]^{2+}$	$[\text{Pb}(\text{H}_2\text{O})_4]^{2+}$		$[\text{Pb}(\text{H}_2\text{O})_5]^{2+}$		$[\text{Pb}(\text{H}_2\text{O})_6]^{2+}$	
	<i>hemi</i>	<i>holo</i>	<i>hemi</i>	<i>holo</i>	<i>hemi</i>	<i>holo</i>
Coulomb	-179.7	-171.4	-206.4	-198.8	-229.0	-224.3
repulsion	103.5	87.5	106.1	91.9	108.2	94.5
polarization	-70.2	-61.2	-71.2	-63.9	-70.4	-64.6
Pb-polarization	-7.4	-1.6	-6.1	-1.2	-6.0	-0.6
charge-transfer	-18.3	-15.8	-18.5	-16.3	-18.2	-16.7
total interaction	-159.7	-153.8	-182.5	-177.7	-200.1	-199.4

tribution favors *holo*-directionality. This is also the case in the tetrahedral and trigonal-bipyramidal $[\text{Pb}(\text{H}_2\text{O})_4]^{2+}$ and $[\text{Pb}(\text{H}_2\text{O})_5]^{2+}$ complexes. Second-order energetic terms (polarization and charge-transfer) therefore account for the stabilization of *hemi*-directed structures in this series of complexes. The polarization energy makes the largest second order stabilizing contribution, with most of the difference between *holo*- and *hemi*-directed conformations arising from polarization of the Pb^{2+} cation. This result can be rationalized, as arranging ligands on one side of the Pb^{2+} cation generates a net electric field at the position of the metal cation whereas field-cancellation arises almost completely from evenly spacing ligands in opposing positions in a *holo*-oriented complex. Indeed, the difference in cation polarization energy between the $[\text{Pb}(\text{H}_2\text{O})_4]^{2+}$ and $[\text{Pb}(\text{H}_2\text{O})_5]^{2+}$ *holo*- and *hemi*-directed complexes is roughly equal to the difference in total binding energy favoring the *hemi*-directed structure. Charge-transfer, too, is non-negligible, and adds a smaller contribution of around 2 kcal/mol favoring *hemi*-directionality. As a relatively large basis set is used, BSSE distortion of the charge transfer energy is small (of the

order of 0.01 kcal/mol) so the estimates are considered to be reliable. It should be noted that RVS total interaction energies are expected to differ slightly to the Gaussian03 binding energies reported above, as the complexation energy in RVS calculations is calculated as the difference between the isolated monomers in their supermolecular conformations, rather than in their gas phase-optimized geometries as reported in Tables 1 and 2.

Parametrization of SIBFA. An accurate representation of cation polarization and charge transfer, then, is key to modeling the energies of Pb^{2+} complexes. While such terms are missing from simpler force fields, detailed approaches such as SIBFA are better equipped for such tasks. The adjustable parameters required in SIBFA to describe the separate energetic contributions of eq 1 were therefore fitted using RVS results for the $[\text{Pb}(\text{H}_2\text{O})]^{2+}$ complex as a function of Pb–O distance. The results of this fitting are shown graphically in Figure 4 and are tabulated in Table 4. A good fit was possible for all terms, although the polarization energy deviates slightly from the corresponding RVS value at short-range. The cation quadrupolar polarization energy terms were fitted similarly using a $[\text{Pb}(\text{H}_2\text{O})_2]^{2+}$ complex with H_2O ligands placed opposite one another to neutralize the field generated at the Pb^{2+} position, leaving a field gradient. An acceptable fit was again achieved as a function of the Pb–O bond length.

Validation of the SIBFA parameters was performed by modeling the six complexes of *holo*- and *hemi*-directed $[\text{Pb}(\text{H}_2\text{O})_4]^{2+}$, $[\text{Pb}(\text{H}_2\text{O})_5]^{2+}$, and $[\text{Pb}(\text{H}_2\text{O})_6]^{2+}$ presented in Figure 3. As shown in Table 5, very satisfactory agreement is observed between SIBFA and RVS results. All contributions are well represented, including the

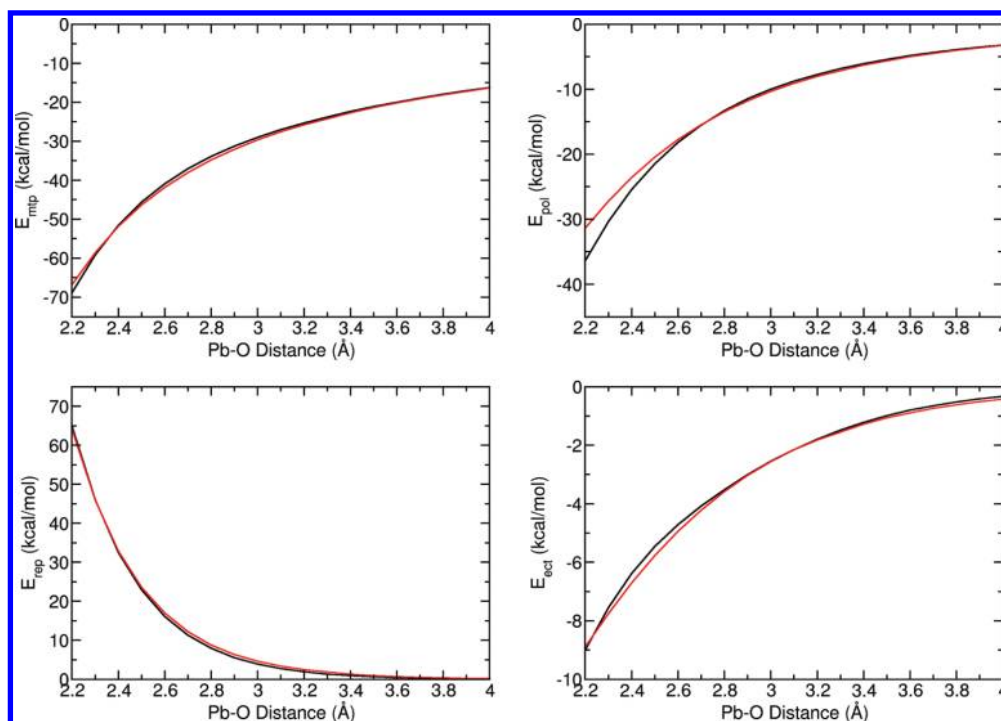
**Figure 4.** RVS (black) vs SIBFA (red) Coulomb (top left), polarization (top right), repulsion (bottom left) and charge-transfer (bottom right) energies as a function of the Pb–O distance in $[\text{Pb}(\text{H}_2\text{O})]^{2+}$.

Table 4. SIBFA vs RVS Data at Different Pb–O Separations r in the $[\text{Pb}(\text{H}_2\text{O})]^{2+}$ Complex^a

r (Å)	$E(\text{mtp})$		$E(\text{rep})$		$E(\text{pol})$		$E(\text{ct})$	
	RVS	SIBFA	RVS	SIBFA	RVS	SIBFA	RVS	SIBFA
2.2	-68.89	-66.88	65.08	64.25	-36.46	-31.43	-9.01	-8.90
2.3	-59.11	-58.54	45.98	45.87	-30.34	-27.20	-7.55	-7.75
2.4	-51.55	-51.82	32.44	32.84	-25.43	-23.56	-6.38	-6.71
2.5	-45.63	-46.34	22.87	23.57	-21.45	-20.44	-5.46	-5.77
2.6	-40.91	-41.81	16.09	16.95	-18.18	-17.76	-4.71	-4.94
2.7	-37.09	-38.02	11.31	12.22	-15.51	-15.47	-4.08	-4.21
2.8	-33.94	-34.81	7.94	8.82	-13.31	-13.50	-3.52	-3.58
2.9	-31.29	-32.06	5.57	6.38	-11.50	-11.81	-3.01	-3.03
3.0	-29.02	-29.69	3.90	4.62	-10.01	-10.36	-2.55	-2.56
3.1	-27.05	-27.61	2.73	3.35	-8.77	-9.11	-2.15	-2.16
3.2	-25.32	-25.78	1.91	2.44	-7.73	-8.04	-1.80	-1.81
3.3	-23.78	-24.23	1.33	1.87	-6.83	-7.18	-1.48	-1.55
3.4	-22.39	-22.70	0.93	1.29	-6.08	-6.31	-1.22	-1.27
3.5	-21.14	-21.38	0.65	0.94	-5.43	-5.62	-0.99	-1.07
3.6	-20.00	-20.19	0.45	0.69	-4.85	-5.02	-0.80	-0.89
3.7	-18.95	-19.11	0.31	0.50	-4.36	-4.50	-0.65	-0.74
3.8	-17.99	-18.12	0.22	0.37	-3.93	-4.04	-0.52	-0.62
3.9	-17.10	-17.21	0.15	0.27	-3.54	-3.64	-0.42	-0.51
4.0	-16.28	-16.36	0.11	0.20	-3.20	-3.28	-0.33	-0.43

^a Coulomb (E_{mtp}), repulsion (E_{rep}), polarization (E_{pol}), and charge-transfer (E_{ct}) energies (kcal/mol) are compared at each separation.

Table 5. Comparison of RVS Energy Decomposition and Corresponding SIBFA Energetic Components for $[\text{Pb}(\text{H}_2\text{O})_n]^{2+}$ Complexes in *holo*- and *hemi*-Directed Conformations (kcal/mol)^a

	$[\text{Pb}(\text{H}_2\text{O})_4]^{2+}$				$[\text{Pb}(\text{H}_2\text{O})_5]^{2+}$				$[\text{Pb}(\text{H}_2\text{O})_6]^{2+}$			
	RVS		SIBFA		RVS		SIBFA		RVS		SIBFA	
	<i>hemi</i>	<i>holo</i>	<i>hemi</i>	<i>holo</i>	<i>hemi</i>	<i>holo</i>	<i>hemi</i>	<i>holo</i>	<i>hemi</i>	<i>holo</i>	<i>hemi</i>	<i>holo</i>
Coulomb (E_{mtp})	-179.7	-171.4	-181.1	-172.8	-206.4	-198.8	-210.0	-201.9	-229.0	-224.3	-235.9	-229.2
repulsion (E_{rep})	103.5	87.5	103.1	85.1	106.1	91.9	106.9	91.1	108.2	94.5	111.8	95.3
pol. RVS (E_{pol}^*)	-70.2	-61.2	-64.9	-59.7	-71.2	-63.9	-67.6	-63.2	-70.4	-64.6	-67.7	-64.8
pol. VL (E_{pol})	-65.3	-54.2	-67.6	-55.0	-64.3	-54.5	-66.1	-56.1	-61.1	-53.1	-63.3	-55.9
Pb-polarization	-7.4	-1.6	-5.3	0.0	-6.1	-1.2	-4.5	-0.1	-6.0	-0.6	-4.7	0.0
charge-transfer (E_{ct})	-18.3	-15.8	-17.0	-16.4	-18.5	-16.3	-18.1	-17.5	-18.2	-16.7	-19.0	-18.2
total	-159.7	-153.8	-162.7	-159.1	-182.5	-177.7	-187.3	-184.5	-200.1	-199.4	-206.4	-207.9

^a The polarization energy is shown before iteration (Pol. RVS/ E_{pol}^*) and after iteration (Pol. VL/ E_{pol}) to self-consistency of the electric field (see text for details). In column 1, headings describe the RVS contributions to the total interaction energy, with values in parentheses indicating which term in SIBFA this corresponds to (see eq 1).

polarization energy of each system before and after iteration of the complex's electric field to self-consistency. The "RVS" polarization energy is the same polarization energy reported in Tables 3 and 4 and arises from the polarization of each monomer due to the unperturbed electric field created by each surrounding *unpolarized* monomer. The 'variation-like' (VL) value arises from polarization of each monomer by the electric field generated by each of the surrounding *polarized* monomers. This second value requires an iterative, self-consistent procedure in SIBFA. Not only are absolute values of the different contributions of the interaction energy in good quantitative agreement with RVS results, but importantly the relative energies of the different *holo*- and *hemi*-directed structures are also in good agreement. The *hemi*-directed structures are successfully predicted to be more stable in both the $[\text{Pb}(\text{H}_2\text{O})_4]^{2+}$ and $[\text{Pb}(\text{H}_2\text{O})_5]^{2+}$ complexes, while the iso-energetic $[\text{Pb}(\text{H}_2\text{O})_6]^{2+}$ *holo*- and *hemi*-directed structures are predicted to be separated by 1.5 kcal/mol only. SIBFA is therefore able to encapsulate the energetic processes underlying stabilization of *hemi*-directed structures, at least for the Pb–H₂O complexes

presented, by means of an accurate treatment of cation polarization.

As a final point of interest, QM/MM calculations were used to investigate whether point charge representations of the H₂O ligands, of the type widely applied in classical force fields, were sufficient to induce a characteristic *hemi*-directed shift in lone-pair distribution such as that visible in Figure 1. These QM/MM calculations were performed with Gaussian03 at the B3LYP level of theory. Pb²⁺ was again represented using the small-core pseudopotential and aug-cc-pVTZ basis-set, while Kollman⁷⁷ charges fitted to B3LYP/aug-cc-pVTZ data were used to represent ligand atoms. As shown in Figure 5, a *hemi*-directed arrangement of point charges representing the H₂O ligands is insufficient to significantly displace the Pb²⁺ lone pair basin in the $[\text{Pb}(\text{H}_2\text{O})_5]^{2+}$ complex. The ELF analysis of the QM-represented cation therefore shows an essentially spherical lone-pair distribution, with the cation nucleus located roughly at the center. This result demonstrates that, while an accurate treatment of cation polarization is vital to describe Pb-ligand interactions, a realistic representation

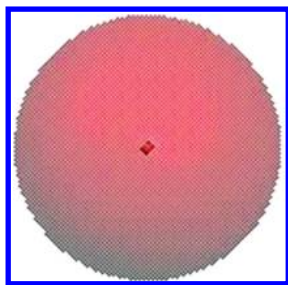


Figure 5. ELF isosurface ($\eta = 0.8$) showing the $V(\text{Pb})$ basin in QM/MM representation of *hemi*-directed $[\text{Pb}(\text{H}_2\text{O})_5]^{2+}$ structure: the use of classical force field point charges to represent H_2O ligands results in only a very slight distortion of the QM Pb^{2+} $V(\text{Pb})$ basin from the spherical distribution observed for the *holo*-directed structure.

of ligand electrostatics and other energetic contributions must also be maintained.

Conclusions

A series of hydrated Pb^{2+} complexes have been used to study the underlying physical origins of the stabilization of *holo*- or *hemi*-directed arrangements of ligands from an energy decomposition perspective. The RVS analysis demonstrates that the stabilization of *hemi*-directed structures can be explained largely in terms of cation polarization arising from the electric field (and to a lesser extent from the field gradient) generated by the hemitropic ligand arrangement. Corresponding *holo*-directed structures, while reducing ligand–ligand repulsion, lead to small or zero net electric fields and, consequently, lower polarization energy.

Parameters fitted for the SIBFA force field have demonstrated that an accurate representation of the cation polarization can encapsulate the *hemi*-stabilizing effect. Good quantitative agreement was achieved in total complex binding energies and in relative *holo*- and *hemi*-directed complex energies in the series of hydrated Pb clusters studied. Extension of the force field to additional ligand types is currently underway, allowing molecular mechanics investigation of the interactions of Pb^{2+} cations within complexes^{11,76} and biological systems⁷⁸ and aiding in the search for selective chelating agents that can be used *in vivo* to cure lead poisoning.

Finally, it is found that the level of theory employed, in particular the choice between large-core and small-core PPs, can have a significant impact on calculated binding energies and especially on RVS values at short ligand– Pb^{2+} distances. RVS results suggest that this discrepancy arises primarily from artifacts associated with the overlap of ligand electronic density and that arising from the large-core PPs at short-range. Small-core PPs therefore represent a safer choice for studies of this kind.

Acknowledgment. The computations reported in this work were performed using resources from GENCI (CINES/IDRIS), Grant Nos. 2009-075009 and x2010075027, and from the Centre de Ressources Informatiques de Haute Normandie (CRIHAN, Rouen, France), Grant Nos. 1998053 and 2008011. Financial support from the French National

Research Agency (ANR) on project SATURNIX (No. 2008-CESA-020) is acknowledged.

Supporting Information Available: The pseudopotentials used in this work. Also included is a figure demonstrating ELF analysis of $[\text{Pb}(\text{CO})_5]^{2+}$ and $[\text{Pb}(\text{CO})_6]^{2+}$ complexes, and additional details relating to the SIBFA force field. This information is available free of charge via the Internet at <http://pubs.acs.org>.

References

- (1) Patterson, C. C. *Arch. Environ. Health* **1965**, *11*, 344–360.
- (2) Casas, J.; Fernández, J. S. C.; Sordo, J. *Lead: Chemistry, Analytical Aspects, Environmental Impact and Health Effects*; Elsevier: New York, 2006.
- (3) Finkelstein, Y.; Markowitz, M. E.; Rosen, J. F. *Brain Res. Rev.* **1998**, *27*, 168–176.
- (4) Wang, S.; Zhang, J. *J. Environ. Res.* **2006**, *101*, 412–418.
- (5) Bergdahl, I. A.; Grubb, A.; Schütz, A.; Desnick, R. J.; Wetmur, J. G.; Sassa, S.; Skerfving, S. *Pharmacol. Toxicol.* **1997**, *81*, 153–158.
- (6) Gourlaouen, C.; Parisel, O. *Ang. Chem. Intern.* **2007**, *46*, 553–556.
- (7) Ghering, A. B.; Miller Jenkins, L. M.; Schenck, B. L.; Deo, S.; Mayer, R. A.; Pikaart, M. J.; Omichinski, J. G.; Godwin, H. A. *J. Am. Chem. Soc.* **2005**, *127*, 3751–3759.
- (8) Godwin, H. A. *Curr. Op. Chem. Bio.* **2001**, *5*, 223–227.
- (9) Jaffe, E. K.; Martins, J.; Li, J.; Kervinen, J.; Dunbrack, R. L. *J. Biol. Chem.* **2001**, *276*, 1531–1537.
- (10) Gourlaouen, C.; Parisel, O. *Int. J. Quantum Chem.* **2008**, *108*, 1888–1897.
- (11) van Severen, M.-C.; Gourlaouen, C.; Parisel, O. *J. Comput. Chem.* **2010**, *31*, 185–194.
- (12) Shimoni-Livny, L.; Glusker, J. P.; Bock, C. W. *Inorg. Chem.* **1998**, *37*, 1853–1867.
- (13) van Severen, M.-C.; Piquemal, J.-P.; Parisel, O. *Chem. Phys. Lett.* **2009**, *478*, 17–19.
- (14) Stevens, W. J.; Fink, W. *Chem. Phys. Lett.* **1987**, *139*, 15–22.
- (15) Piquemal, J.-P.; Williams-Hubbard, B.; Fey, N.; Deeth, R. J.; Gresh, N.; Giessner-Prettre, C. *J. Comput. Chem.* **2003**, *24*, 1963–1970.
- (16) Gresh, N.; Claverie, P.; Pullman, A. *Theor. Chim. Acta* **1984**, *66*, 1–20.
- (17) Gresh, N. *J. Comput. Chem.* **1995**, *16*, 856–882.
- (18) Piquemal, J.-P.; Gresh, N.; Giessner-Prettre, C. *J. Phys. Chem. A* **2003**, *107*, 10353–10359.
- (19) Gresh, N.; Cisneros, G. A.; Darden, T. A.; Piquemal, J.-P. *J. Chem. Theory Comput.* **2007**, *3*, 1960–1986.
- (20) Gresh, N.; Stevens, W. J.; Krauss, M. *J. Comput. Chem.* **1995**, *16*, 843–855.
- (21) Gresh, N. *J. Phys. Chem. A* **1997**, *101*, 8680–8694.
- (22) de Courcy, B.; Pedersen, L. G.; Parisel, O.; Gresh, N.; Silvi, B.; Pilmé, J.; Piquemal, J.-P. *J. Chem. Theory Comput.* **2010**, *6*, 1048–1063.
- (23) (a) Antony, J.; Piquemal, J. P.; Gresh, N. *J. Comput. Chem.* **2005**, *26*, 1131–1147. (b) Gresh, N.; Piquemal, J.-P.; Krauss, M. *J. Comput. Chem.* **2005**, *26*, 1113–1130.

- (24) (a) Roux, C.; Gresh, N.; Perera, L.; Piquemal, J.-P.; Salmon, L. *J. Comput. Chem.* **2007**, *28*, 938–957. (b) Jenkins, L. M. M.; Hara, T.; Durell, S. R.; Hayashi, R.; Inman, J. K.; Piquemal, J.-P.; Gresh, N.; Appella, E. *J. Am. Chem. Soc.* **2007**, *129*, 11067–11078. (c) Foret, F.; de Courcy, B.; Gresh, N.; Piquemal, J.-P.; Salmon, L. *Bioorg. Med. Chem.* **2009**, *17*, 7100–7107. (d) Gresh, N.; Audiffren, N.; Piquemal, J.-P.; de Ruyck, J.; Ledecq, M.; Wouters, J. *J. Phys. Chem. B* **2010**, *114*, 4884–4895.
- (25) de Courcy, B.; Piquemal, J.-P.; Garbay, C.; Gresh, N. *J. Am. Chem. Soc.* **2010**, *132*, 3312–3320.
- (26) de Courcy, B.; Piquemal, J.-P.; Gresh, N. *J. Chem. Theory Comput.* **2008**, *4*, 1659–1668.
- (27) MacKerell, A. D., Jr.; Bashford, D.; Bellott, M.; Dunbrack, R. L., Jr.; Evansck, J. D.; Field, M. J.; Fischer, S.; Gao, J.; Guo, H.; Ha, S.; Joseph-McCarthy, D.; Kuchnir, L.; Kuczera, K.; Lau, F. T. K.; Mattos, C.; Michnick, S.; Ngo, T.; Nguyen, D. T.; Prodhom, B.; Reiher, I. W. E.; Roux, B.; Schlenkrich, M.; Smith, J. C.; Stote, R.; Straub, J.; Watanabe, M.; Wiorcikiewicz-Kuczera, J.; Yin, D.; Karplus, M. *J. Phys. Chem. B* **1998**, *102*, 3586–3616.
- (28) Weiner, S. J.; Kollman, P. A.; Case, D. A.; Singh, U.; Ghio, C.; Alagona, G.; Profeta, S., Jr.; Weiner, P. *J. Am. Chem. Soc.* **1984**, *106*, 765–784.
- (29) Ponder, J. W.; Wu, C.; Ren, P.; Pande, V. S.; Chodera, J. D.; Schnieders, M. J.; Haque, I.; Mobley, D. L.; Lambrecht, D. S.; DiStasio, R. A.; Head-Gordon, M.; Clark, G. N. I.; Johnson, M. E.; Head-Gordon, T. *J. Phys. Chem. B* **2010**, *114*, 2549–2564.
- (30) Åstrand, P.-O.; Linse, P.; Karlström, G. *J. Chem. Phys.* **1995**, *191*, 195–202.
- (31) Handley, C. M.; Hawe, G. I.; Kell, D. B.; Popelier, P. L. A. *Phys. Chem. Chem. Phys.* **2009**, *11*, 6365–6376.
- (32) Schaeffer, C. E.; Jorgensen, C. K. *Mol. Phys.* **1965**, *9*, 401–412.
- (33) Larsen, E.; Mar, G. N. L. *J. Chem. Educ.* **1974**, *51*, 633–640.
- (34) Frisch, M. J.; Trucks, G. W.; Schlegel, H. B.; Scuseria, G. E.; Robb, M. A.; Cheeseman, J. R.; Montgomery, J. A., Jr.; Vreven, T.; Kudin, K. N.; Burant, J. C.; Millam, J. M.; Iyengar, S. S.; Tomasi, J.; Barone, V.; Mennucci, B.; Cossi, M.; Scalmani, G.; Rega, N.; Petersson, G. A.; Nakatsuji, H.; Hada, M.; Ehara, M.; Toyota, K.; Fukuda, R.; Hasegawa, J.; Ishida, M.; Nakajima, T.; Honda, Y.; Kitao, O.; Nakai, H.; Klene, M.; Li, X.; Knox, J. E.; Hratchian, H. P.; Cross, J. B.; Bakken, V.; Adamo, C.; Jaramillo, J.; Gomperts, R.; Stratmann, R. E.; Yazyev, O.; Austin, A. J.; Cammi, R.; Pomelli, C.; Ochterski, J. W.; Ayala, P. Y.; Morokuma, K.; Voth, G. A.; Salvador, P.; Dannenberg, J. J.; Zakrzewski, V. G.; Dapprich, S.; Daniels, A. D.; Strain, M. C.; Farkas, O.; Malick, D. K.; Rabuck, A. D.; Raghavachari, K.; Foresman, J. B.; Ortiz, J. V.; Cui, Q.; Baboul, A. G.; Clifford, S.; Cioslowski, J.; Stefanov, B. B.; Liu, G.; Liashenko, A.; Piskorz, P.; Komaromi, I.; Martin, R. L.; Fox, D. J.; Keith, T.; Al-Laham, M. A.; Peng, C. Y.; Nanayakkara, A.; Challacombe, M.; Gill, P. M. W.; Johnson, B.; Chen, W.; Wong, M. W.; Gonzalez, C.; Pople, J. A. *Gaussian 03, Revision E.01*; Gaussian, Inc., Wallingford, CT, 2004.
- (35) Becke, A. D. *J. Chem. Phys.* **1993**, *98*, 5648–5652.
- (36) Lee, C.; Yang, R.; Parr, W. G. *Phys. Rev. B* **1988**, *37*, 785–789.
- (37) Küchle, W.; Dolg, M.; Stoll, H.; Preuss, H. *Mol. Phys.* **1991**, *74*, 1245–1263.
- (38) Ross, R. B.; Powers, J. M.; Atashroo, T.; Ermler, W. C.; LaJohn, L. A.; Christiansen, P. A. *J. Chem. Phys.* **1990**, *93*, 6654–6670.
- (39) Stevens, W. J.; Krauss, M.; Basch, H.; Jasien, P. G. *Can. J. Chem.* **1992**, *70*, 612–630.
- (40) Schuchardt, K. L.; Didier, B. T.; Elsethagen, T.; Sun, L.; Gurumoorhi, V.; Chase, J.; Li, J.; Windus, T. L. *J. Chem. Inf. Model.* **2007**, *47*, 1045–1052.
- (41) Feller, D. *J. Comput. Chem.* **1996**, *17*, 1571–1586.
- (42) Gourlaouen, C.; Piquemal, J.-P.; Parisel, O. *J. Chem. Phys.* **2006**, *124*, 174311.
- (43) Stevens, W. J.; Basch, H.; Krauss, M. *J. Chem. Phys.* **1984**, *81*, 6026–6033.
- (44) Peterson, K. A. *J. Chem. Phys.* **2003**, *119*, 11099–11112.
- (45) Zhao, Y.; Schultz, N. E.; Truhlar, D. G. *J. Chem. Theory Comput.* **2006**, *2*, 364–382.
- (46) Zhao, Y.; Truhlar, D. G. *Theor. Chem. Acc.* **2007**, *120*, 215–241.
- (47) Stephens, P. J.; Devlin, F. J.; Chabalowski, C. F.; Frisch, M. J. *J. Phys. Chem.* **1994**, *98*, 11623–11627.
- (48) Perdew, J. P.; Burke, K.; Ernzerhof, M. *Phys. Rev. Lett.* **1996**, *77*, 3865–3868.
- (49) Perdew, J. P.; Burke, K.; Ernzerhof, M. *Phys. Rev. Lett.* **1997**, *78*, 1396–1396.
- (50) Purvis, G. D. *J. Chem. Phys.* **1982**, *76*, 1910–1918.
- (51) Scuseria, G. E.; Janssen, C. L.; Schaefer, H. F. *J. Chem. Phys.* **1988**, *89*, 7382–7387.
- (52) Pople, J. A.; Head-Gordon, M.; Raghavachari, K. *J. Chem. Phys.* **1987**, *87*, 5968–5975.
- (53) Head-Gordon, M.; Pople, J. A.; Frisch, M. J. *J. Chem. Phys. Lett.* **1988**, *153*, 503–506.
- (54) Møller, C.; Plesset, M. S. *Phys. Rev.* **1934**, *46*, 618–622.
- (55) Schmidt, M. W.; Baldridge, K. K.; Boatz, J. A.; Elbert, S. T.; Gordon, M. S.; Jensen, J. H.; Koseki, S.; Matsunaga, N.; Nguyen, K. A.; Su, S.; Windus, T. L.; Dupuis, M.; Montgomery, J. A., Jr. *J. Comput. Chem.* **1993**, *14*, 1347–1363.
- (56) Kitaura, K.; Morokuma, K. *Int. J. Quantum Chem.* **1976**, *10*, 325–340.
- (57) Bagus, P. S.; Hermann, K.; Bauschlicher, C. W. *J. Chem. Phys.* **1984**, *80*, 4378–4386.
- (58) Becke, A. D.; Edgecombe, K. E. *J. Chem. Phys.* **1990**, *92*, 5397–5403.
- (59) Noury, S.; Krokidis, X.; Fuster, F.; Silvi, B. *Comput. Chem. (Oxford)* **1999**, *23*, 597–604.
- (60) Savin, A.; Nesper, R.; Wengert, S.; Fässler, T. F. *Angew. Chem.* **1997**, *109*, 1892–1918.
- (61) Savin, A.; Nesper, R.; Wengert, S.; Fässler, T. F. *Ang. Chem. Intern.* **1997**, *36*, 1808–1832.
- (62) Silvi, B.; Savin, A. *Nature* **1994**, *371*, 683–686.
- (63) Savin, A.; Silvi, B.; Coionna, F. *Can. J. Chem.* **1996**, *74*, 1088–1096.
- (64) Piquemal, J.-P.; Pilmé, J.; Parisel, O.; Gérard, H.; Fourré, I.; Bergès, J.; Gourlaouen, C.; De la Lande, A.; van Severen, M.-C.; Silvi, B. *Int. J. Quantum Chem.* **2008**, *108*, 1951–1969.
- (65) Noury, S.; Krokidis, X.; Fuster, F.; Silvi, B. TopMod Package. This package is available on the web site of the Laboratoire

- de Chimie Théorique, Université Pierre et Marie Curie (UMR 7616, CNRS—Paris 6 -UPMC), URL: www.lct.jussieu.fr (see the personal home page of Prof. B. Silvi) Accessed July 2010.; 1997.
- (66) Pilmé, J.; Piquemal, J.-P. *J. Comput. Chem.* **2008**, *29*, 1440–1449.
- (67) Piquemal, J.-P.; Chevreau, H.; Gresh, N. *J. Chem. Theory Comput.* **2007**, *3*, 824–837.
- (68) Vigne-Maeder, F.; Claverie, P. *J. Chem. Phys.* **1988**, *88*, 4934–4948.
- (69) Garmer, D. R.; Stevens, W. J. *J. Phys. Chem.* **1989**, *93*, 8263–8270.
- (70) (a) Foster, J. M.; Boys, S. F. *Rev. Mod. Phys.* **1960**, *32*, 300–302. (b) Boys, S. F. *Rev. Mod. Phys.* **1960**, *32*, 296–299.
- (71) Piquemal, J.-P.; Chelli, R.; Procacci, P.; Gresh, N. *J. Phys. Chem. A* **2007**, *111*, 8170–8176.
- (72) Gresh, N.; Claverie, P.; Pullman, A. *Int. J. Quantum Chem.* **1986**, *29*, 101–118.
- (73) Murrell, J. N.; Randic, M.; Williams, D. R. *Proc. R. Soc. London* **1965**, *284*, 566–581.
- (74) (a) Gresh, N.; Claverie, P.; Pullman, A. *Int. J. Quantum Chem.* **1985**, *28*, 757–771. (b) Gresh, N.; Claverie, P.; Pullman, A. *Int. J. Quantum Chem.* **1982**, *22*, 199–215.
- (75) Gresh, N.; Policar, C.; Giessner-Prettre, C. *J. Phys. Chem. A* **2002**, *106*, 5660–5670.
- (76) Gourlaouen, C.; Gérard, H.; Piquemal, J.-P.; Parisel, O. *Chem.—Eur. J.* **2008**, *14*, 2730–2743.
- (77) Singh, U. C.; Kollman, P. A. *J. Comput. Chem.* **1984**, *5*, 129–145.
- (78) van Severen, M.-C.; Piquemal, J.-P.; Parisel, O. *J. Phys. Chem. B* **2010**, *114*, 4005–4009.

CT1004005